Electrical and Electronic Engineering: 2011; 1(1): 42-48
DOI: 10.5923/j.eee.20110101.07

8×8 Near-Field Focused Circularly Polarized Cylindrical DRA Array for RFID Applications

S. H. Zainud-Deen*, H. A. Malhat, K. H. Awadalla

Department of Electronics and Electrical Communications Engineering, Faculty of Electronic Engineering, Menoufiya University, Egypt

Abstract The design of 8×8 near-field focused circularly polarized dielectric resonator antenna (DRA) array for fixed RFID reader applications at 5.8GHz is presented. The proposed antenna array consists of 64-element of circular dielectric resonator antennas (CDRA) with two orthogonal feeding probes located inside the CDRA element. A single element CDRA with supporting arms used as a building block of the array provide good impedance matching and circular polarization at 5.8GHz. The perforation technique is used for the supporting arms to reduce the manufacturing complexities in the DRA mounting over the ground plane. The sequential feeding technique is used to improve the gain and circular polarization bandwidth of the single element and the array. The characteristics of the near-field focused array are introduced compared to that of uniformly phased array. The finite integral technique and the finite element method are used to compute the array performance

Keywords DRA, RFID, Fixed Reader antenna, Sequential Feeding

1. Introduction

RFID technological aspects and limits are becoming more and more important in devising new electronic products[1]. Problems that may arise with conventional RFID readers include:1) the reader may detect tags that are not in the reader coverage area, and 2) the tags may be located adjacent to the reader antenna thus blocking its field. This can lead to errors in customer purchases or errors in verification that an item is in a specific physical location (e.g., baggage on a specific cart)[2-4]. The RFID reader antenna is an important component in RFID systems and it has been designed with circularly polarized (CP) operation. CP for the reader antennas in transmission is preferred because the tag antenna (which is linearly polarized) will receive enough power from the transmitter irrespective of its orientation. A CP antenna with a low profile, small size, lightweight, high gain, and high front-to-back ratio is required in a portable RFID reader [5-7]. Recently, fixed-reader antennas are becoming more complex microstrip patch arrays with high gain, and a relatively narrow beam and low side lobe level[8-10]. In some applications, tags may be located in the near-field region of the reader antenna array not in its far-field region as is usually the case in standard communication system. Therefore, a reader antenna array exhibiting a near-field (NF) focused radiation, which is able to maximize the field amplitude in a size-limited spot within the antenna near-field region, while not affecting the field strength far from the antenna (far-field region) is needed. Recently, NF-focusing has attracted major interest due to its potential applications in near-field sensing and imaging microscopy[11-13]. NF- focusing is used in RFID to increase the field incident on the tags at allowed effective isotropic radiated power (EIRP)[14]. In this paper, an 8×8 NF-focused cylindrical DRA phased array with supporting arms for fixed RFID reader at 5.8GHz is proposed. The performance parameters of the NF-focused array are compared with that of uniform phased array. The finite integration technique (FIT)[15] is used to optimize and analyze the antenna array performance parameters such as reflection coefficient, radiation pattern and antenna gain. The finite element method (FEM) is used to validate the results [16].

* Corresponding author:
er_honida@yahoo.com（H. A. Malhat）
Published online at http://journal.sapub.org/eee

2. Numerical Results

Figure 1 shows the geometry of a single cylindrical dielectric resonator antenna (CDRA) with two feed probes excitation. The CDRA with dielectric constant ε_r of 10.2 is used[17]. It has a radius '*a*' of 5.9 mm and a height 'H_d' of 8.3mm. The CDRA is designed to operate around 5.8GHz. Two coaxial probes with a radius 0.25 mm located off the center by distance d_f of 5.1 mm and height h_f of 3.9 mm. The two probes are parallel and located at similar positions on two orthogonal diameters and the feeding is arranged such that the two probes have a phase difference of 90^o. Because of the fabrication complexity of DRA over ground plane, four supporting arms having rectangular shape are connected

with the CDRA above the ground plane. Perforated structure was proposed in[38] to overcome the mounting problems of the DRA over the ground plane and more manual effort in the alignment of the DRA with the feeding structure especially for arrays. The technique of perforating a dielectric sheet eliminates the need to position and bond individual DRA elements in an array. Perforations create different effective dielectric permittivity and make the fabrication of DRA arrays feasible. The perforations result in lowering the effective dielectric constant for the region between the DRA elements. The CDRA element is made from one piece of dielectric material; with a perforated bonding dielectric rods and completely eliminating all the rest of the dielectric material. The dielectric rods have low dielectric constant and thin enough to avoid guiding waves around the design frequency of the element itself. The effective dielectric constant, ε_{reff}, of the perforated material can be calculated from[18]

$$\varepsilon_{reff} = \varepsilon_r (1-\alpha) + \alpha, \text{ and } \alpha = \frac{\pi R_p^2}{2\left(\sqrt{3}/4\right) S_p^2} \quad (1)$$

where R_p is the radius of the air holes, and S_p is the center to center separation distance of the holes. The holes forming the perforation are only one line centered along the axis of the ribbon forming the supporting arm. Thus, the supporting arms are used to reduce the fabrication complexity while keeping the same radiation characteristic as arm free element [18-20]. The dimensions of the supporting arms are width W_p= 4 mm, and thickness H_p=1 mm. The supporting arms are perforated by incorporating air holes in the arms. The air holes have equal radii, R_p=1.2 mm and center to center separation S_p=3R_p. The CDRAs with supporting arms are mounted on square ground plane with edge length 'G' of 35.15 mm.

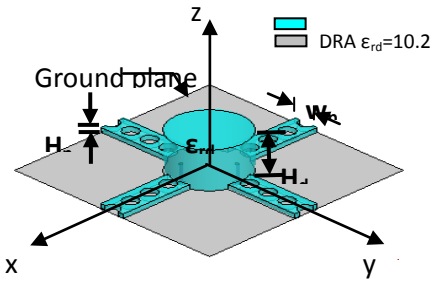

a. 3-D view

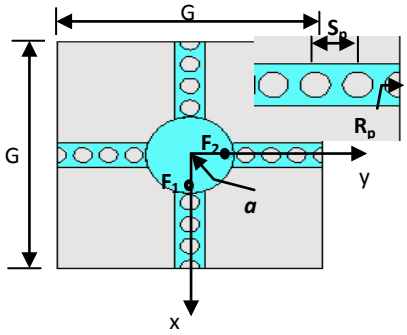

b. Top view

Figure 1. The geometry of a circularly polarized CDRA with supporting arms.

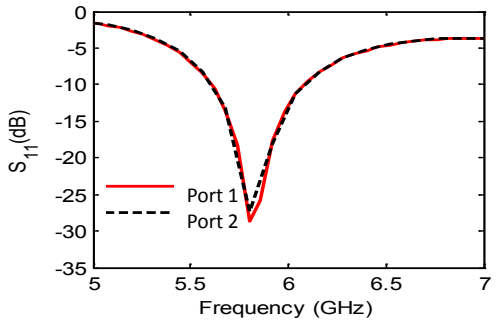

a. The return loss

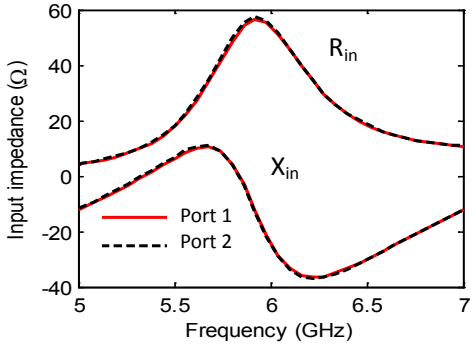

b. The input impedance

Figure 2. The return loss and input impedance versus frequency of the CDRA with supporting arms.

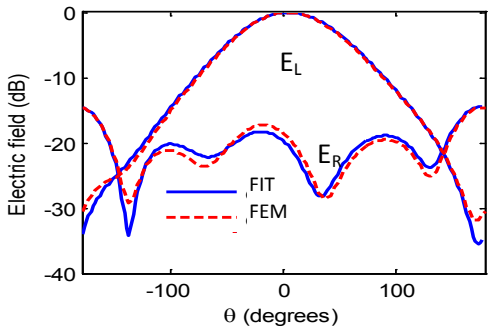

a. x-z plane

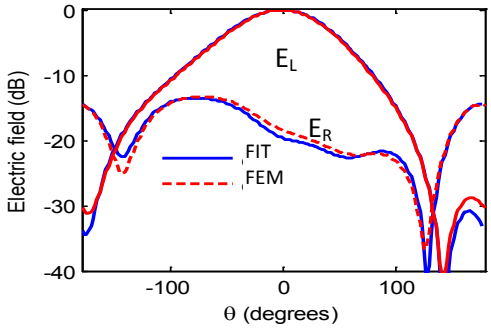

b. y-z plane

Figure 3. The simulated radiation pattern components of the single element at 5.8GHz.

Figure 2 shows the simulated return loss, S11, at the two ports of the feeding pins of the CDRA with perforated supporting arms against the frequency. The two ports produced the same performance due to their similarity as is expected. Good impedance matching is obtained with impedance

bandwidth extending from 5.62GHz to 6.12GHz for S11 < -10dB. The simulated radiation pattern components, left hand polarization, EL, and right hand polarization, ER, of the single element at 5.8GHz in x-z plane and y-z plane are shown in Figure. 3. Asymmetrical radiation pattern is obtained with high cross-polarization level due to the coupling effect between the excitation orthogonal probes, as well as the asymmetrical positioning and asymmetrical phase of the feeds with respect to the two planes. Good agreement is obtained between the results calculated by FEM and FIT techniques. The main polarization (EL) is within -10dB level in a beam of about 100° width centered at the 0° direction. The cross polarization (ER) level is more than -10dB relative to the main polarization (EL) within the circular polarization beam (100°). These results indicate good performance of this dielectric resonator antenna relative to the RFID application.

The axial ratio at the normal axis, φ= θ=0o, versus frequency is shown in Figure. 4a. The antenna provides circular polarization with minimum value of 1.9dB at 5.8GHz with a relatively wide axial ratio bandwidth (AR< 3dB) of the order of 40.74%. The antenna gain at the normal axis over the operating band is shown in Figure. 4b. The gain at the normal axis is 7.15dB at 5.8GHz and nearly constant within 0.5dB over the RFID frequency band (5.65- 5.95GHz).

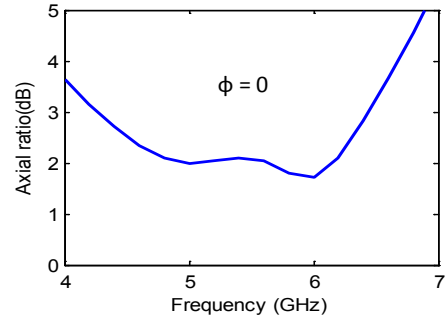

a. Axial ratio

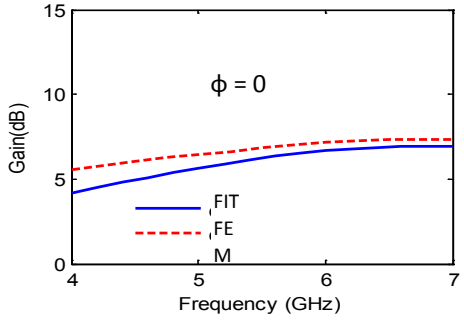

b. Gain

Figure 4. The simulated axial ratio and antenna gain versus frequency of the single element CDRA with supporting arms.

A pair-unit consists of two CDRA elements are shown in Figure. 5. The elements are fed with equal powers from orthogonal feed points F1, F2, F3 and F4. The elements are out of phase from each other by 90o phase shift, and rotated in position by -90o with F2 is kept in phase with F3. The distance G between the elements is 35.16 mm (0.68λ) to reduce the mutual coupling between the elements. The return losses for ports 1 and port 3 are computed for the pair- unit as shown in Figure. 6. The four curves are coincident as expected. These return loss curves are done when the other three ports are matched. Good impedance matching is obtained over the impedance band width from 5.58GHz to 6.1GHz. The polarization components patterns are depicted in two planes φ=0, and φ=90o as shown in Figure. 7.

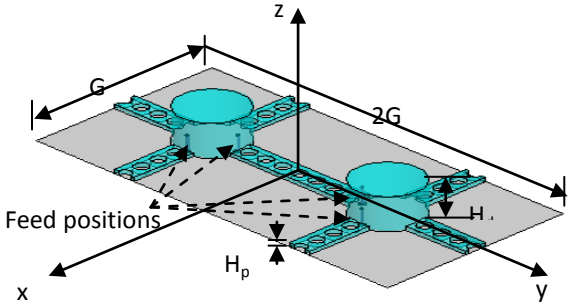

a. 3-D view.

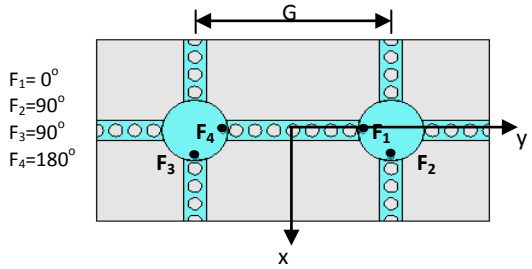

b. Top view.

Figure 5. The constriction of the pair-unit CDRA array with supporting arm.

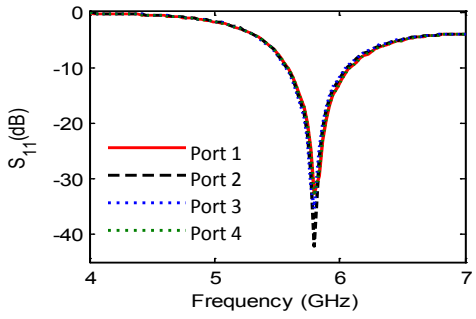

a.

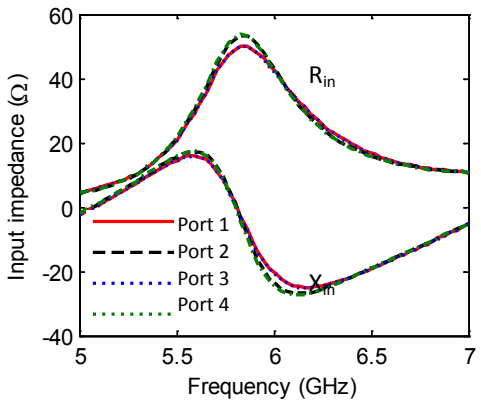

b.

Figure 6. The return losses and input impedance versus frequency of the pair-unit CDRA with supporting arms.

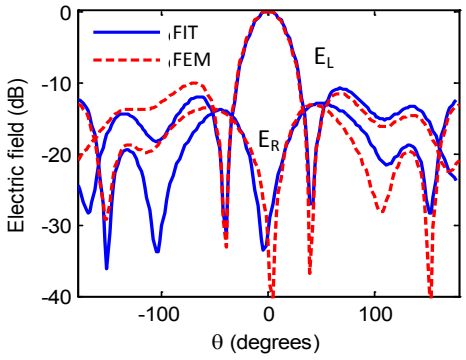

a. x-z plane

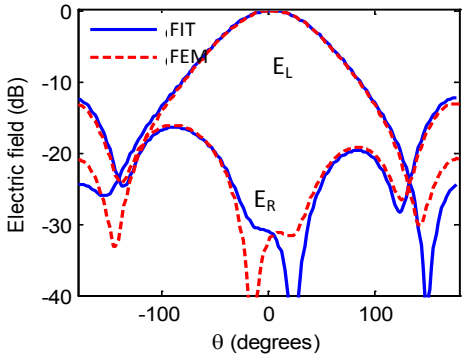

b. y-z plane

Figure 7. The simulated polarization components pattern of the pair-unit CDRA with supporting arms at 5.8GHz.

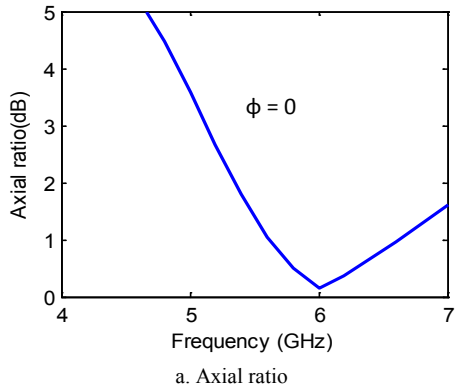

a. Axial ratio

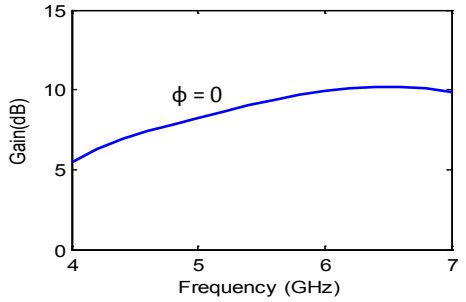

b. Gain

Figure 8. The simulation of the improvement in the axial ratio and antenna gain versus frequency of the pair-unit CDRA with supporting arms.

A directional pattern with high EL/ER ratio is obtained. The cross-polarization component ER is more that 30dB lower than the in-phase component EL in the z-direction. The axial ratio versus frequency for the pair- unit at φ= θ=0 is shown in Figure. 8a. This configuration shows an improvement in the axial ratio bandwidth for AR< 3dB covering most of the RFID band, with value of 0.51dB at frequency f=5.8GHz. The antenna gain variation versus frequency at φ=0 and θ=0 is shown in Figure. 8b. An improvement in the antenna gain is obtained along the frequency band with value equal 9.87dB at frequency f=5.8GHz. The gain varies between 8dB to 10dB within the RFID band. This variation of the gain is acceptable within the considered band.

The sequential feeding technique is applied to the pair-units of the CDRA elements in order to improve the circular polarization bandwidth (axial ratio bandwidth) and gain of the previously proposed pair-unit. The geometry of four sequentially feed CDRA elements in 2×2 sub-array is shown in Figure. 9. The elements in one diagonal are 90o out of phase and rotated -90o in orientation relative to the elements in the other diagonal as shown in Figure. 9. The simulated circular polarization radiation pattern components, EL and ER, are shown in Figure. 10. As the number of elements has increased, the patterns become more directional with narrower main lobe. The front-to-back ratio has improved significantly with a null in the backward direction for the desired polarization in this case. On the other hand, the cross polarization level has gone down significantly in the forward direction but is not that low in the reverse direction. The axial ratio versus frequency is shown in Figure. 11a. The sub-array provides an extremely broadband axial ratio bandwidth (AR< 1dB all over the frequency band from 4-7GHz). The improvement in sub-array antenna gain versus frequency is presented in Figure. 11b providing high gain of 12.8dB at 5.8GHz.

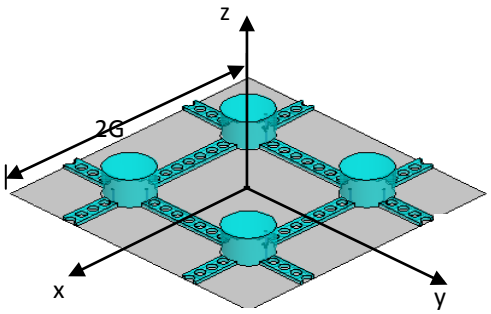

a. 3-D view.

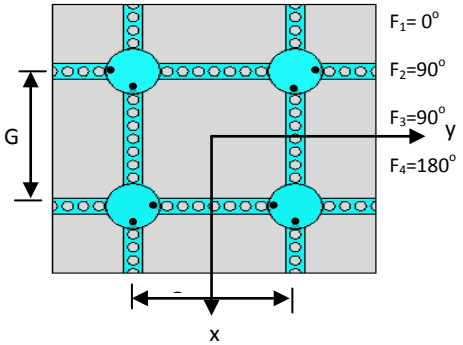

b. Top view.

Figure 9. The geometry of sub-array CDRA array with supporting arms.

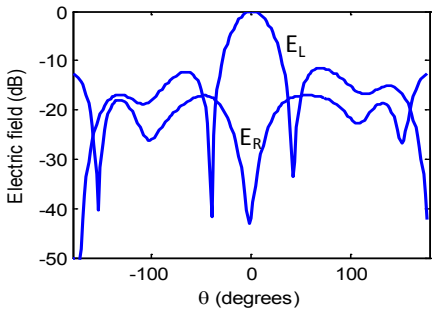

a. x-z plane

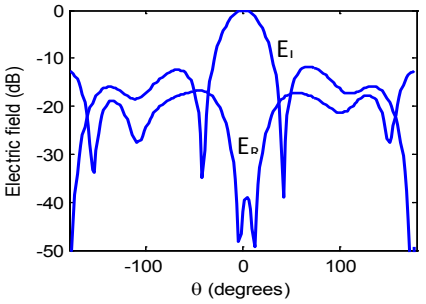

b. y-z plane

Figure 10. The simulated polarization pattern components of the sub-array CDRA with supporting arms at 5.8GHz.

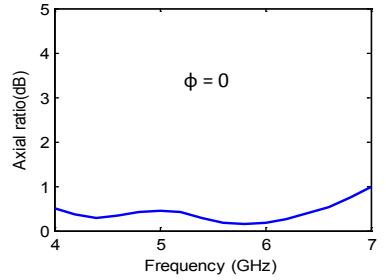

a. Axial ratio

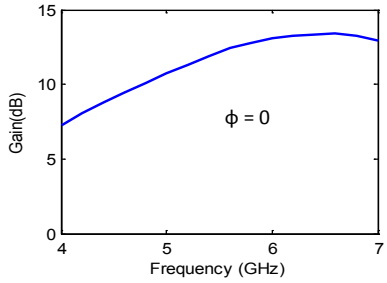

b. Gain

Figure 11. The simulated the axial ratio and antenna gain versus frequency of the sub-array CDRA with supporting arms.

Finally, the 8 ×8 RFID reader antenna array consists of four 4×4 sub-arrays of CDRA with supporting arms is shown in Figure. 12. The total dimensions of the array are L×L= 28.13 × 28.13cm^2. The antenna array aperture is placed in the (x, y) plane and (x_i, y_i) are the position coordinates of the ith element. The phase of the feeding currents has been adjusted to maximize the radiated field at a distance R_o=40cm (The assumed boundary for the far field is $2L^2/\lambda$ = 2×((28.13)^2/5.17) = 306.11cm) from the antenna aperture. For the NF- focused phased array, the phase shift for the ith element can be calculated from[21]

$$\varphi_i = \frac{2\pi}{\lambda}\left(\sqrt{x_i^2 + y_i^2 + R_o^2} - R_o\right) \tag{2}$$

The beamwidth between 3-dB points in the focal plane is defined as the array spot size. The spot size area radius, W of a NF-focused planar array depends on the inter-element distance, array size and geometry, required focal length and phase profile at the antenna aperture[22,23]

$$W = 0.8868\ R_o \cdot \frac{\lambda}{L} \tag{3}$$

For L=28.13cm, R_o=40cm, and λ_o=5.17cm, W=1.26 λ_o (which is W= 6.52cm). The Poynting vector which is equal to the cross product of electric field, $\bar{E}$, by the complex conjugate of the magnetic field, $\hat{H}$. The magnitude of its real part is the active power density while the magnitude of its imaginary part is the reactive power density[22]. Adding the phase shift to the array elements results in focusing both the active and reactive power density at the focal plane (the plane which include the focus point). The ratio between the active power density and the reactive power density is very large (about 256). Thus, only the active radiated power density will be taken into account and is given by

$$S = \left\| \mathrm{Re}\left(\vec{S}\right) \right\| = \left\| \mathrm{Re}\left(\vec{E} \times \vec{H}^*\right) \right\| \tag{4}$$

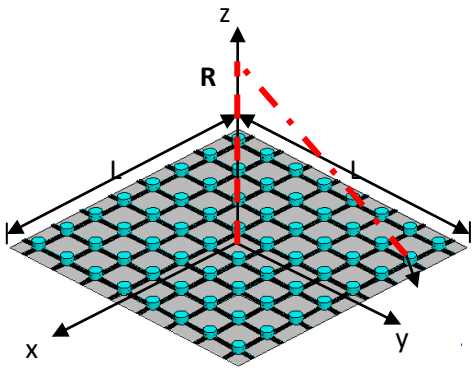

Figure 12. The geometry of the proposed 8 ×8 RFID reader antenna array consists of 4 sub-array of CDRA with supporting arms.

The equivalent plane wave power density p are defined from the E-field or the H-field as follows[21]

$$p = S_e = \frac{\left\|\vec{E}_x\right\|^2 + \left\|\vec{E}_y\right\|^2 + \left\|\vec{E}_z\right\|^2}{\eta_o}, \tag{5}$$

$$or \quad p = S_h = \eta_o \cdot \left(\left\|\vec{H}_x\right\|^2 + \left\|\vec{H}_y\right\|^2 + \left\|\vec{H}_z\right\|^2\right)$$

where η_o=377Ω. The normalized power density distribution in the x-y plane for the uniformly phased array compared to that of the NF-focused array is used to introduce the effect of focusing as shown in Figure. 13. The power density of the NF-focused antenna array decreases rapidly from the focal point than that of the uniformly phased array. A contour plot of the normalized power density in the transverse plane for both the uniformly phased and NF-focused array are shown in Figure. 14. The -3dB contour curve of the NF-focused array exhibits a diameter of about 8cm. Contour plots of the normalized power density in the x-z plane is plotted in Figure. 15.

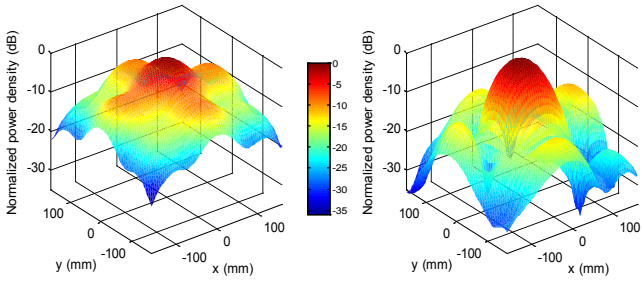

a. Uniformly phased array b. NF- focused array

Figure 13. A 3-D plot of the simulated normalized power density of the 8×8 CDRA with supporting arms for both the uniformly phased and NF-focused array.

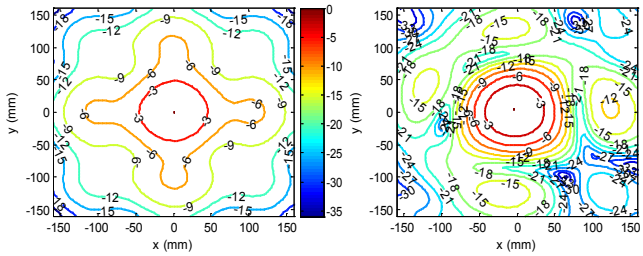

a. Uniformly phased array b. NF- focused array

Figure 14. A contour plot of the simulated normalized power density of the 8×8 CDRA with supporting arms in the transverse plane for both the uniformly phased and NF-focused array.

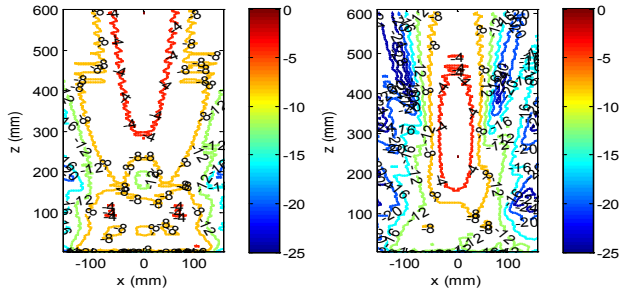

a. Uniformly phased array b. NF- focused array

Figure 15. A contour plot of the simulated normalized power density of the 8×8 CDRA with supporting arms in the x-z plane at y=0 for both the uniformly phased and NF-focused array.

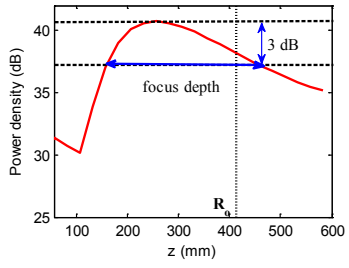

Figure 16. Simulated radiated power density along the axial direction for the NF-focused CDRA array with supporting arms.

Figure 16 shows the power density variation along the z-axis from the antenna aperture of the NF-focused array. The 3-dB focused depth of the array is 31.2cm along the array axis. The AR in 20 × 20cm^2 area of the transverse plane at focal point 40cm away from the NF array aperture is shown in Figure. 17. The NF-focused array exhibits focused circular polarization in area around the focal point less than that for the uniformly phased array.

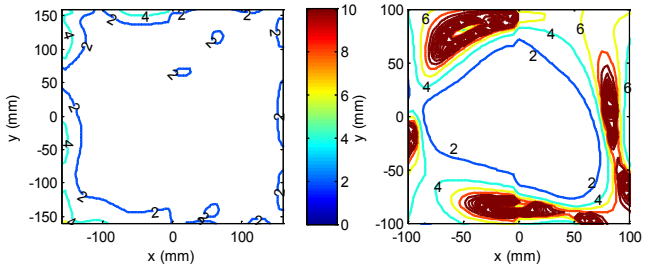

a. uniformly phased array b. NF focused array

Figure 17. Contour plot of the simulated axial ratio in an 20 ×20cm^2 area at R_o= 40cm from the antenna aperture.

The variations of the normalized power density along x-axis and y-axis for uniformly phased array and NF- focused array are shown Figure. 18. The side lobe level, SLL, in the 32 × 32cm2 area around the focal point is less than -13.5dB while -5.82dB for the uniformly phased array. Approximately the same field distributions in the far- field region for the uniformly phased array are obtained in the near field region for the NF-focused array due to the phase correction of each element in the array.

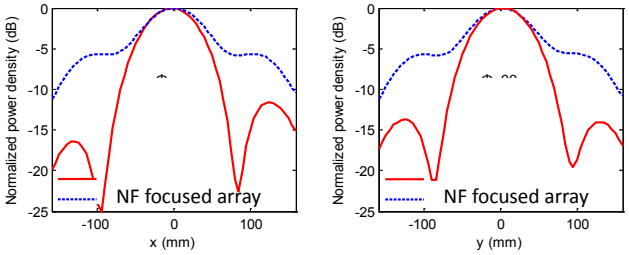

a . x-z plane b. y-z plane

Figure 18. Simulated normalized power density along the transverse direction at R_o= 40cm from the antenna aperture.

3. Conclusions

The performance of the proposed NF- focused CDRA array compared with uniformly phased CDRA array have been presented. The NF-focused CDRA array is maximizing the radiated power at a limited size spot of radius 6.5cm in the focal plane at 40cm from the array aperture with a 3-dB focus depth of 31.2cm along the axis normal to the array aperture. The NF- focused array produces a far-field like pattern in the near–field at the focal plane. Thus the near field focused array will improve the performance of the reader antenna for the RFID application, and consequently improve the detectability of the tagged objects in the near field.

REFERENCES

[1] K. Finkenzeller, RFID handbook: radio-frequency identification fundamentals and applications, 2nd Ed., Wiley & Sons, Inc., New Jersey, USA, 2004.

[2] R. Bhochhibhoya, Mobile tag reading in a multi-reader RFID environment, M. Sc. Thesis, Pokhara University, Ne-

pal, India, 2005.

[3] W. Arts, E.D. Mulder, B. Preneel, G.A. Vandenbosch, and I. Verbauwhede, "Dependence of RFID reader antenna design on read out distance," IEEE Trans. on Antennas and Propag., vol. 56, no. 12, pp. 3829-3837, December 2008.

[4] S. H. Zainud-Deen, Hend A. Malhat, and K. H. Awadalla, "Circular polarized dielectric resonator antenna for portable RFID reader using a single feed," International Journal of Radio Frequency Identification & Wireless Sensor Networks, vol. 1, no.1, 2011.

[5] S. H. Zainud-Deen, Hend A. Malhat, and K. H. Awadalla, "Octafilar helical antenna for handheld UHF-RFID reader," International Journal of Radio Frequency Identification & Wireless Sensor Networks, vol. 1, no.1, 2011.

[6] C.F. Tseng, C.L. Huang, and C.H. Hsu, "A wideband planar inverted-F dielectric resonator antenna for RFID system applications," Microwave and Opt. Tech. Letters, vol. 48, no. 7, pp. 1302-1305, July 2006.

[7] Z. Sun, S.S. Zhong, X.R. Tang, and K.D. Chen, "Low-side lobe circular-polarized microstrip array for 2.45 GHz RFID readers," Microwave and Opt. Tech. Letters., vol. 50, no. 9, pp. 2235-2237, September 2008.

[8] M. Abbak, and I. Tekin, "RFID coverage extension using microstrip-patch antenna array," IEEE Antennas and Propag. Magazine, vol. 51, no.1, pp. 185-191, February 2009.

[9] M. Bogosanovie, and A.G. Williamson, "Microstrip antenna array with a beam focused in the near field zone for application in noncontact microwave industrial inspection," IEEE Trans. on Instruments and Measurements, vol. 56, no. 6, pp. 2186-2495, December 2007.

[10] J.T. Loane, and S. Lee, "Gain optimization of near field focusing array for hyperthermia applications," IEEE Trans. on Microwave Theory and Techniques, vol. 37, no. 10, pp. 1629-1635, October 1989.

[11] F.R.L. Silva, M.T. de Melo, and M.D. Lourenc¸ O. Junior, "Coplanar antenna array design with stubs over dipoles for RFID applications," Microwave and Opt. Tech. Letters, vol. 50, no. 4, pp. 877-879, April 2008.

[12] H.T. Chou, T.M. Hung, N.N. Wang, H.H. Chou, C. Tung, and P. Nepa, "Design of a near field focused reflectarray antenna for 2.4 GHz RFID reader applications ," IEEE Trans. Antennas Propag., vol. 59, no. 3, pp. 1013-1018, March 2011.

[13] H.T. Chou, C. Tung, T.M. Hung, H.H. Chou, and P. Nepa, "Design of a near field focused reflectarray antenna for RFID reader applications, " in Proc. IEEE Antennas and Propag. Soc. Int. Symp., vol. 48, Toronto, Canada, June 2010.

[14] S. H. Zainud-Deen, Hend A. Malhat, and K. H. Awadalla, "Near-field focused DRA Array for fixed RFID reader," International Journal of Radio Frequency Identification & Wireless Sensor Networks, vol. 1, no.1, 2011.

[15] R. Siragusa, P. Lemaître-Auger, and S. Tedjini, "Tuneable near-field focused circular phase-array antenna for 5.8-GHz RFID applications," IEEE Antennas and Wireless Propag. Letters, vol. 10, pp. 33-36, January 2011

[16] R. Schuhmann, T. Weiland, W.H. Schilders, E.J. Maten, and S.H. Houben, "Recent advances in finite integration technique for high frequency applications," Scientific Computing in Electrical Engineering, vol. 4, pp. 46-57, 2004.

[17] J. L. Volakis, A. Chatterjee, L. C. Kempel, Finite element method for electromagnetic : antennas, microwave circuits, and scattering applications, IEEE Press, Piscataway, NJ,1998.

[18] M.T. Sebastian, Dielectric materials for wireless communication, Elsevier Ltd., 2008.

[19] R. Chair, A. A. Kishk, and K. F. Lee, "Experimental investigation for wideband perforated dielectric resonator antenna," Electronic Letters, vol. 42, no. 3, pp. 137-139, Feb. 2006

[20] Y. Zhang, and A. A. Kishk, "Analysis of dielectric resonator antenna arrays with supporting perforated rods," 2nd European Conf. on Antennas and Propag., (EuCAP 2007), pp. 1-5, 2007.

[21] M. Hansishi, and H. Takazawa, "Broad band circularly polarized planar array composed of a pair of dielectric resonator antennas," Electronics Letters, vol. 21, no. 10, pp. 437-438, May 1985.

[22] R. C. Hansen, "Focal region characteristics of focused array antennas," IEEE Trans. Antennas Propag., vol. 33, no. 12, pp. 1328-1337, December 1985.

[23] Y. Adanel, M. Wongl, C. Dale', and J. Wiartl, "Near field power density characterization of radio base station antennas using spherical harmonics optimization techniques," European Conference on Wireless Technology, Amsterdam, Holland, pp. 121-124, 2004.

[24] A.J. Fenn, "On the radial component of the electric field for a monopole phased array antenna focused in the near zone," IEEE Trans. Antennas Propag., vol. 40, no. 6, pp. 723-727, June 1992.